UNCECOMP 2015
1st ECCOMAS Thematic Conference on
Uncertainty Quantification in Computational Sciences and Engineering
M. Papadrakakis, V. Papadopoulos, G. Stefanou (eds.)
Crete Island, Greece, 25–27 May 2015

EVALUATION AND UNCERTAINTY QUANTIFICATION OF BIFURCATION DIAGRAM: LANDING GEAR, A CASE STUDY

I. Tartaruga[1], J. E. Cooper[2], M. H. Lowenberg[2], P. Sartor[2] and Y. Lemmens[3]

[1]University of Bristol
Queens Building, University Walk, Bristol, BS8 1TR, United Kingdom
e-mail: irene.tartaruga@bristol.ac.uk,

[2]University of Bristol
Queens Building, University Walk, Bristol, BS8 1TR, United Kingdom
e-mail: {J.E.Cooper, M.Lowenberg, pia.sartor}@bristol.ac.uk

[3] Siemens
Interleuvenlaan 68, 3001 Leuven, Belgium
e-mail: yves.lemmens@siemens.com

Keywords: Bifurcation Analysis, Hopf bifurcation, Uncertainty Quantification, Sensitivity Analysis, Surrogate Model, Singular Value Decomposition

Abstract. *Bifurcations are features of dynamical systems and occur when a small change in a system parameter results in a sudden qualitative change in the system behaviour. Such events can occur in linear and non-linear systems. The analysis of this phenomenon is challenging in the presence of non-linearity even for simple systems since they lack the properties and principles common to linear systems, e.g. the superposition principle. In the last few decades, numerical methodologies have been developed in order to efficiently determine bifurcation diagrams. Such techniques include continuation, normal form analysis, harmonic balance, and more recently branch and bounds methods. However, very little work has been considered for quantification of uncertain non-linear systems. In this paper, a methodology is provided to propagate parametric uncertainties and define bounds for the bifurcation diagrams taking into account the factors that most influence the behaviour of the analysed dynamical system. To this end, the developed methodology includes sensitivity analysis and uncertainty quantification. The methodology exploits numerical continuation methods, (high order) singular value decompositions, interval analysis and Bayesian approach, which is adopted in the Kriging method to develop surrogate models . The proposed method is validated considering a complex non-linear system from the aeronautical field: a landing gear (LG) system. The LG system has been the subject of several deterministic studies predicting the occurrence of shimmy, which is a self-excited oscillation dangerous for the integrity of the aircraft. This phenomenon arises from Hopf bifurcations. The case study explores the effects of uncertainty on this phenomenon.*

1 INTRODUCTION

Bifurcation is a phenomenon that is common in several dynamical systems and can be described as a sudden qualitative change in the system behaviour due to small variations in systems parameters. A common misunderstanding of bifurcations is to relate them only to physical systems modelled taking into account non-linearity. In fact this phenomenon can exhibit itself also in linear systems: all physical systems have non-linearity, which can be more or less important. The kind of effect the bifurcation can imply is influenced by the presence of non-linearities. This paper is focused on a particular effect that can occur only in non-linear systems: the Limit Cycle Oscillation (LCO). LCOs are isolated closed trajectories characterized by periodical solutions for the states of the systems and can be *stable* or *unstable* if the neighbouring trajectories approach them or not, respectively. This differentiation is not always true and there can be the case of *half-stable* LCOs. LCOs can be generated after a particular bifurcation, called a Hopf bifurcation, that is one of the bifurcations of fixed points (along with pitchfork bifurcation, saddle-node, transcritical bifurcations). Hopf bifurcations can occur in systems with at least two degrees of freedom (DoFs); mathematically, it occurs when the real part of a pair of complex eigenvalues, of the Jacobian matrix of the linearised system, changes sign as a parameter varies. There are three different kinds of Hopf bifurcation depending on the behaviour of the system after the bifurcation point: supercritical, subcritical and degenerate.

Stable LCOs are of particular interest in science because they model systems that can exhibit self-sustained oscillations, oscillations that are not due to external force but are generated by the system itself. Some of these fascinating phenomena characterize our life each day: the beating of a heart, the daily rhythms in human body temperature and hormone secretion, chemical reactions that oscillate spontaneously [1]. With regard to the engineering field, *stable* LCOs are often the cause of dangerous events: self-exciting vibrations in bridges and wings, and oscillation in landing gear, known as *shimmy*. In particular, *shimmy* is a phenomenon exhibited not only by landing gear systems, but by all the systems with wheels that interact with the ground.

Bifurcation analysis is a subject of interest in many fields, such as mathematics and engineering, and there are many different approaches developed to evaluate and describe bifurcation diagrams. Bifurcation diagrams can be evaluated by adopting a pure *Monte Carlo random search*, *numerical* and *experimental continuation*, exploiting *non-linear normal forms* and *branch and bounds methods*. All these methods, apart from *non-linear normal forms*, find a numerical solution. The *normal forms* are a significant mathematical method that theoretically fulfils the requirement to find an analytical solution to non-linear problems, among which are the identification of bifurcation diagrams and/or backbone curves [2]. All the stated methods can be adopted to identify equilibrium branches of the bifurcation diagrams (including steady-state bifurcation points, such as pitchfork and saddle-node bifurcations, and Hopf bifurcations). However, not all of them solve periodical solutions (e.g. Limit Cycle Oscillation (LCO)): *continuation*, *experimental* and, ideally, pure *Monte Carlo random search* and *non-linear normal forms* can be exploited. In the case of periodical solutions, Harmonic Balance methods have also been diffusely adopted for the identification of LCOs in the aereolastic and aerodynamics fields [3] [4] [5].

Dealing with dangerous phenomena occurring after Hopf bifurcations, such as *shimmy*, it is important to define confidence intervals that take into account the presence of uncertainty. Uncertainty is always present in life and in process modelling can be classified as model (form), parametric (aleatory and epistemic, i.e. irreducible and reducible uncertainty) and/or predictive

uncertainty. In this regard, in a design process two general approaches can be adopted, which are shown in Figure 1: deterministic and non deterministic approaches. They are intrinsically different concerning the treatment of uncertainty [6]. Deterministic approaches consider the presence of uncertainty just at the end of the analysis using the so called 'safety factor', i.e. the system responses are obtained considering the modelled system as 'true'. This assumption can cause an over/under-designed system if the safety factor is too high or low. Non deterministic approaches consider the presence of uncertainty from the beginning and so a more robust design can be achieved. They can employ stochastic and/or interval approaches depending on the uncertainty typology, i.e. aleatory and epistemic. In real systems both these kinds of uncertainties are present and so it is desirable to develop approaches that sensibly combine stochastic and interval methodologies. Deterministic approaches are attractive in their simplicity, but unacceptable in the presence of significant randomness and lack of knowledge. Finally, adopting the non deterministic approaches, the robustness of the achieved result can be strongly limited by the required time, which is a parameter that significantly limits the applicability of methodologies that could work well on paper. It is for this reason that in a preliminary design, the analyses are done through the use of simulators, especially in the presence of complex dynamics and/or structures for which experiments can be very time expensive and/or impracticable.

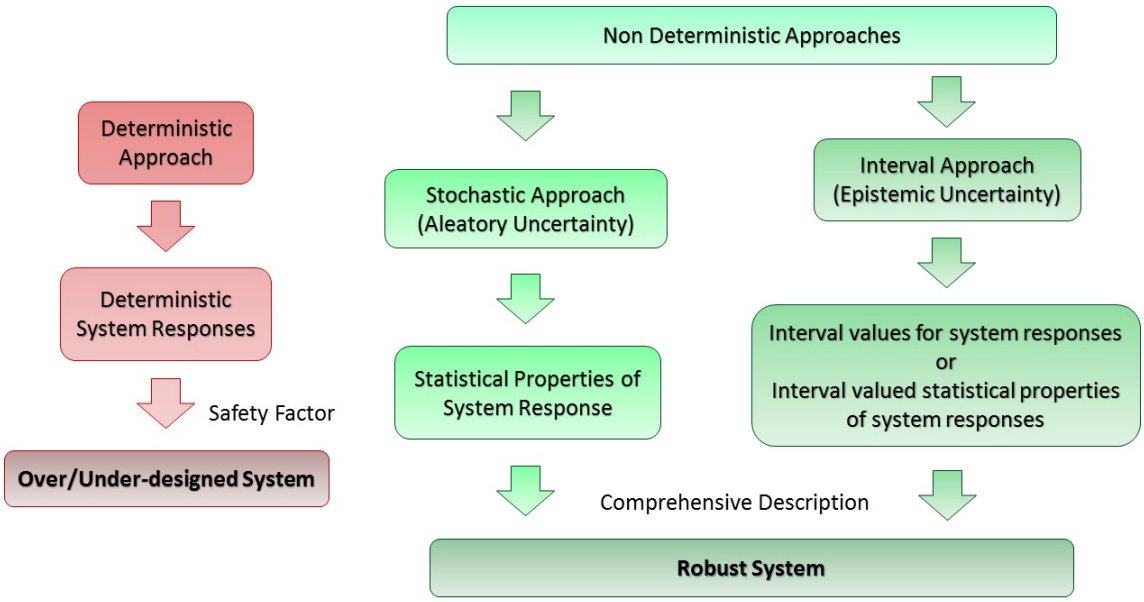

Figure 1: Approaches in a design process.

In the last decade, researchers have been starting to look at the effect of parametric uncertainty in the structural parameters and in composite structures in the *flutter* occurrence and in the amplitude and frequency of LCOs, arising beyond the linear *flutter* speed [5] [7] [8] [9] [10] [11] [12].

The aim of this paper is to present a new methodology to ensure a reliable 'structure' through consideration of uncertainties in bifurcation diagrams. The methodology is implemented in Matlab, through the development of a tool that exploits the Dynamical System Toolbox [19], a Matlab interface with AUTO, the software used to perform numerical continuation analyses [15].

The process risk and reliability management considered here is in terms of the definition of confidence bounds for the possible occurrence of LCOs in the presence of parametric uncertainty. These bounds are for delimitation-branches that are the locus of Hopf bifurcation points and that determines subdivision of the interested parameter space. These subdivision are in terms of absence or possible occurrence of LCOs and a full identification is not trivial, even deterministically. The idea to totally deterministically describe the delimitation-branches consists of three main parts:

1. determine a first set of branches of locus of Hopf bifurcation points in the range of interest of parameters;

2. detect possible other Hopf bifurcations that can be isolated from the ones identified in point 1 and are significant to identify the sought delimitation;

3. critically discuss the possible presence of subcritical Hopf bifurcation. Subcritical Hopf bifurcation is a Hopf bifurcation that causes an unstable LCO for values of some parameters that is less of the ones characterizing the starting Hopf bifurcation point. After the unstable LCO, a stable LCO, characterised by high amplitude values, typically occurs. It is apparent that this detection is significant for a robust identification of the sought delimitation.

In this paper, results and discussion for all the stated points are provided. The uncertainty propagation has been performed developing a method that shares the same principles adopted in the technique already been validated by the author in [13]. The technique consists of a new SVD[1]-based methodology and has already been adopted in order to predict gust lengths that cause critical correlated aircraft loads in presence of parametric uncertainty. The novelty in this methodology is in suitably identifying matrices that can capture the 'behaviour' of interest affecting the Interesting Quantities (IQs) and then in constructing surrogate models in terms of coefficients that are extracted applying the SVD. In this paper, new aspects are introduced in the methodology:

– both the singular value decomposition (SVD) and the high order singular value decomposition (HOSVD) are used;

– Sobol' indices (main and total effects) are adopted to perform sensitivity analysis (SA) and describe the importance of each design parameter, identifying which ones to use for the uncertainty quantification (UQ).

The developed technique has been validated using an analytical description of a landing gear system. The case study is the *shimmy* phenomenon, i.e. the LCO to be 'bounded' in the presence of parametric uncertainty.

In section 2, the bifurcation analysis and the analysed branches are first briefly discussed justifying the research; then the present problem and the case study are presented. In section 3 the methodology is presented covering each step. Finally, in sections 4 and 5 the results are given and the conclusions are drawn.

[1]Singular Value Decomposition

2 BIFURCATION ANALYSIS AND PRESENT PROBLEM

In this section, a brief introduction to what is a bifurcation in a dynamical system is first presented; the different methods of analysis are then provided and finally, the occurrence of LCOs as an effect of Hopf bifurcations is presented, introducing the concept of 'shimmy'.

2.1 BIFURCATION AND DYNAMICAL SYSTEMS

The term bifurcation was first introduced by Poincaré to describe the 'splitting' of equilibrium solutions in a family of differential equations. J. Guckenheimer provides the following definition in [14]. *'Given a system of differential equations* [2]

$$\dot{\mathbf{x}} = \mathbf{f_p}\left(\mathbf{x}\right); \qquad \mathbf{x} \in \mathbb{R}^{\mathrm{n}}; \qquad \mathbf{p} \in \mathbb{R}^{\mathbf{k}} \tag{1}$$

depending on the k-dimensional parameter $\mathbf{p}$, then a value $\mathbf{p_0}$ of equation (1) for which the flow of (1) is not structurally stable is a bifurcation value of $\mathbf{p}$.' Guckenheimer himself emphasizes how the definition cannot be completely satisfactory since it requires an extremely detailed study of the flow structure that does not exist in practice. A peculiarity of such a definition is that *a point of bifurcation need not actually represent a change in the topological equivalence class of a flow*, it can represent just a qualitative change. Thus, the bifurcation analysis of a system can be conducted in a qualitative manner without trying to depict a systematic bifurcation theory, which would give rise to difficult technical questions.

A common case in which the change is usually of a topological type is the bifurcation of equilibria (or fixed points). For instance, considering equation (1), bifurcations of that type can occur for equilibrium solutions obtained varying the k-dimensional parameter $\mathbf{p}$. These solutions are given by solving $\mathbf{f_p} = \mathbf{0}$ and their existence is assured by the implicit function theorem if the Jacobian derivative of $\mathbf{f_p}$ with respect to $\mathbf{x}$, i.e. $\mathbf{D_x f_p}$, has no zero eigenvalues. Solutions are given by smooth functions of $\mathbf{p}$ and we will call *branches* of equilibria of (1) the graph representation of each of these solutions. An equilibrium $(\mathbf{x_0}, \mathbf{p_0})$ is called a point of bifurcation if at such a point the Jacobian matrix presents a zero eigenvalue; in fact in this situation the equilibrium point $(\mathbf{x_0}, \mathbf{p_0})$ may belong to several branches of equilibria.

Points of bifurcation can be classified mathematically and/ or qualitatively and the description can be very complex, especially in the presence of 'imperfection', intermediate solutions and chaos. The simplest are the so called bifurcations of fixed points to which belongs the Hopf bifurcation, which is the one of interest in the present paper. Thus, for the sake of simplicity, a brief introduction to bifurcations of fixed points is here covered without describing degenerate cases.

Mathematically, the classification of bifurcations of fixed points is performed looking at the fixed points and in some case at the eigenvalues of the Jacobian matrix, that is obtained linearising the system in the neighbourhood of a fixed point. Moreover, typical dynamics representation, called *'normal forms'*, have been identified according to the degrees of freedom of the system. Qualitatively, the characteristic flows in the phase portrait, caused by the occurrence of a fixed point bifurcation, is considered for the classification. Whatever the dimension of the considered system is, the bifurcation of each fixed point keeps the same qualitative description, with the only exception of the Hopf bifurcation, which can occur just in systems with at least two degrees of freedom. In what follows the categorization of bifurcations of fixed points is provided, giving more details for the *Hopf bifurcation*.

[2] $\mathbf{x}$ is the state vector of the system.

– *Saddle-node bifurcation*, also known as *fold bifurcation* or *turning-point bifurcation*, occurs when fixed points are created and destroyed as a set of parameter $\mathbf{p}$ changes.

– *Transcritical bifurcation* is characterized by the change of stability of a fixed point as $\mathbf{p}$ varies.

– *Pitchfork bifurcation* occurs in systems with some inherent symmetry and stable points tend to appear and disappear in symmetrical pairs. This bifurcation can be of two kinds, *supercritical* and *subcritical*, and are characterized by the presence of a cubic term that is stabilizing and destabilizing, respectively.

– *Hopf bifurcation* can happen just in systems with at least two degrees of freedom. This feature is strictly related to the characterization of such a phenomenon: a change of the sign of real parts of complex eigenvalues, thus the necessity of at least two degrees of freedom is straightforward. In presence of non-linearity, Limit Cycle Oscillations (LCOs) can occur, since Limit Cycles (LCs), isolated closed trajectories characterized by periodical solutions for the states of the systems, are present in the Hopf bifurcation. LCs can be *stable* or *unstable* if the neighbouring trajectories approach them or not, respectively. As the *pitchfork bifurcation*, *Hopf bifurcation* can be either *supercritical* or *subcritical*. The difference between these two bifurcations is in the oscillation that arises. A *supercritical Hopf bifurcation* occurs when only a stable fixed point is present before the destabilization, which occurs increasing a set of parameter $\mathbf{p}$, and a stable LC appears after the destabilization of the fixed point: although the fixed point becomes unstable the trajectory is attracted to a LC that appears just after the bifurcation; thus the response tends to be periodical and the amplitude is limit to a fixed value. In the occurrence of *subcritical Hopf bifurcations*, a stable fixed point and LC with an unstable cycle between them are present before the bifurcation. Increasing $\mathbf{p}$, the amplitude of the unstable cycle becomes zero and engulfs the origin making it unstable: all the trajectories are attracted to the LC that is characterized by large oscillations. It is worth empathizing that the *subcritical Hopf bifurcations* is more dangerous since, unlike the *supercritical Hopf bifurcation*, it is 'irreversible': decreasing the values of $\mathbf{p}$ the fixed point cannot be rendered stable and large oscillation persists [1].

2.2 METHODS TO EVALUATE BIFURCATION DIAGRAMS

Numerical continuation [3] is the method selected to evaluate bifurcation diagrams thanks to its capabilities, which fit what is needed to perform SA and UQ in terms of bifurcation diagrams. The main features of *numerical continuation* are:

– analytical representation of the analysed model is not required.

– simplicity in detecting bifurcation points, such as limit point and Hopf bifurcations.

– periodical branches can be solved applying sophisticated continuation methods.

– limited running time for bifurcation diagrams in two parameters, suitably setting up the constants characterizing the method (e.g. step size, tolerance ...).

[3] AUTO is the software used for the continuation [15].

Numerical continuation is usually restricted to low-dimensional parameters [16] and requires an initial solution to identify equilibrium branches. In order to define confidence bounds for the branch delimiting the area of possible occurrence of LCOs, these drawbacks are not as significant as the ones met if one of the other methods would be adopted:

- A *pure Monte Carlo random search* is a *blind* search of bifurcation diagrams. The model is run for an extremely large number of input values, which are randomly selected and a considerable running time is required even for a bifurcation diagram in only one parameter.

- *Non-linear normal forms* are mathematical tools that help in simplifying the system of non-linear equations, identifying the so called *resonant* and *non-resonant* terms, exploiting *suitable* transformation and assumptions. However, so far the potential of using *non-linear normal forms* has been exerted to fully describe the dynamical behaviour, i.e. identify bifurcation diagrams, only for small systems (for instance two degree of freedom systems).

- *Branch and bound methods* require an analytical description of the dynamical system and the branches are identified in terms of bounds, which can be made tighter and give a guarantee of solution just in terms of exclusion. It is necessary (but not sufficient) for a high compactness of the analytical dynamical system in order to achieve a sensible precision for the solution, which requires a significant running time. Finally, the methods have not yet been adopted for periodical branches.

2.3 PRESENT PROBLEM AND CASE STUDY

In order to define confidence bounds of the bifurcation branch delimiting the region of possible occurrence of LCOs first at least two parameters have to be selected to define the parameter space in which the sought restrictions are to be determined.

The idea to identify these restrictions, for each analysed set of values of parameters of interest, already presented in the introduction, is here shown in detail:

1. A first set of branches of locus of bifurcation points can be determined after having run an equilibrium solution changing the values of one of the two selected parameters, keeping the other constant, and identifying the Hopf bifurcations that occur in the range of interest of the changed parameter. In fact, once the points are identified, a switch to a continuation in terms of both the selected parameters can be done determining a set of pairs of values of the two parameters characterizing Hopf bifurcation points; the solutions obtained as a locus of this point is exactly the sought first set of branch-delimitations. Once these delimitations are identified, are known LCOs to occur in these delimited areas. What needs to be investigated is if some LCOs can occur outside this region: the last two points fulfil this requirement.

2. Look for possible occurrence of Hopf bifurcation for which the values of the selected parameters are outside those characterizing the already identified branches (point 1), i.e. due to Hopf bifurcations from other fixed-point solution branches.

3. Check the possible occurrence of *subcritical* Hopf bifurcation, for which the related LCO is present also at values less than those characterising the selected parameters at the identified branches in 1.

The last two requirements are important since in the presence of one or both the stated phenomena, the delimitation determined accomplishing the first point, does not totally identify the region in which LCO can/cannot occur. These two requirements can be fulfilled doing periodical continuation from the first set of determined branches in terms of the parameter fixed in point 1 for the equilibrium solution. In this way, possible occurrence of LCOs at the stable-equilibria side can be detected and the final delimitations depicted.

The confidence bounds for such a delimitation take into account parametric uncertainty present in the analysed system. Due to the presence of a huge number of parameters in models, SA is needed in order to distinguish the parameters that significantly influence the system from those that do not, before propagating the uncertainty. The SA has been performed in terms of the first set of identified branches.

Since the case study in the present paper is the occurrence of *shimmy* in ground manoeuvres, the adopted landing gear model is here briefly presented contextualizing the presented idea.

The landing gear model is based on the that presented by Howcroft [18] and it is a dual-wheel landing gear in which free-plays and wheel gyroscopic effects are not considered. The deflection of the landing gear structure is modelled in terms of three degrees of freedom (DoFs) (Figure 2) and an additional DoF is introduced for the tyre dynamics. The states are in total 7, since the first three dynamics are of the second order while the last is just of first order. The degrees of freedom are:

1. torsional, ψ, describing the rotation of the wheel/axle assembly about the local axis z;
2. in-plane, δ, expressing the bending of the oleo piston in the side-stay plane. This DoF is approximated as a rotation about a point at a distance L_δ from the axle;
3. out-of-plane, β, describing the rotation on the landing gear about the two attachment points;
4. lateral displacement, λ, characterizing the tyre dynamics, which is modelled adopting the straight tangent model.

Further information on the adopted model is provided in [18], in appendix A the nominal values adopted for the parameters of this model are shown.

Having considered the *shimmy* in the landing gear as the case study, the parameter space, in which the delimitation is determined, is the one covered by the Hopf bifurcations as the forward velocity V and the vertical force F_z vary. In fact, during landing manoeuvres, these two parameters vary considerably:

– the vertical force F_z is the one along the main structure of the landing gear and its variation is strictly related to the loading condition (for instance lift relative to weight during take-off landing or taxing). In the present paper, an upper force limit of $4 \cdot 10^5$ N has been considered.

– the forward velocity V during landing manoeuvre must be in agreement with the certification; tables provided in an ICAO [4] document [17] indicate the specified range of handling speeds for each category of aircraft to perform the manoeuvres specified. These speed

[4] International Civil Aircraft Organization

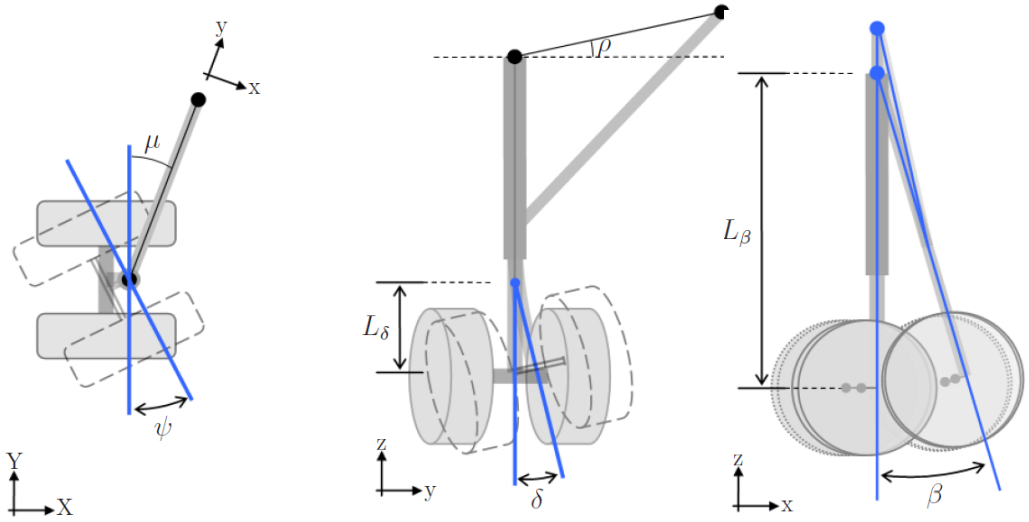

Figure 2: Torsional ψ, lateral δ and longitudinal β degree of freedoms characterising the adopted landing gear model [18]. (XYZ) and (xyz) are the global and local coordinate systems, respectively.

ranges have been assumed for use in calculating airspace and obstacle clearance requirements for each procedure. Taking into account the information provided by ICAO, and the speed at threshold V_{at}v for an airline jet, based on 1.3 times stall speed in the landing configuration at maximum certificated landing mass, a range of interest $0 - 100$ m/s for the forward velocity V has been considered in the analysis.

3 METHODOLOGY

Figure 3 presents the flow process chart of the tool in which the methodology to define confidence bounds for the sought delimitation-branches is implemented. This tool allows the development of a suitable sampling plane for both SA and UQ, run AUTO, perform bifurcation analysis, systematically discuss the influence of parameters on the analysed landing gear model adopting the Sobol' indices as sensitivity metrics and then perform UQ in terms of parameters 'significant' for the system.

In the following subsections, the sensitivity metrics, the method to perform UQ and the adopted error metrics are presented.

3.1 SENSITIVITY ANALYSIS

SA has its origin in the design of experiments (DOE), which was introduced in order to evaluate the input/output (I/O) relation in the presence of variation in factors. Indeed, the definition provided by Saltelli [20] for SA reflects such a feature: '*Sensitivity analysis* studies the relationships between information flowing in and out of the model'. The pattern adopted by both SA and DOE consists of selecting first the factors to be varied in the experiments (physical or numerical), secondly in accomplishing the experiments and finally in picking out suitable statistic tools for the analyses of the data. SA has two main features: it describes how variations in the output can be caused by variations in factors and it analyses which kind of influence the factors have on the system; it does not identify which are the causes of particular outputs. The SA has a significant role in the increment of the level of confidence of a model, a problem raised from the

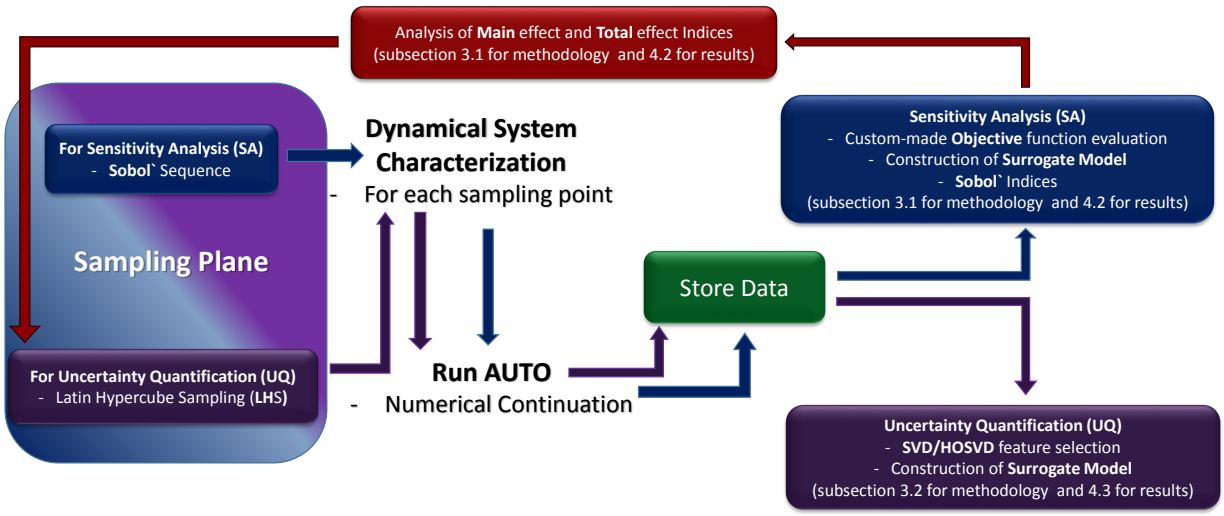

Figure 3: Flow process chart of the tool developed to perform SA and UQ in terms of bifurcation diagrams using AUTO.

presence of uncertainty, which can be model (form), parametric (aleatory and epistemic) and/or predictive [12]: SA is directly correlated to and is a means to cope with the *uncertainty*.

As remarked by Saltelli [20] there is not a '*universal recipe*' that explains how to conduct a SA and which measures should be adopted. The decision for the method and sensitivity measures to be adopted depends on the particular problem, model and accepted computational cost: only experience and engineering judgement can lead to a more efficient pattern or, in other words, to the strategy that implies lower computational cost, which is a general indicator of efficiency and can be described as the number of model evaluations needed for the analysis. In the analysed problem, sensitivity metrics that capture non-linear dynamical behaviour and high order interaction are desirable and for this reason the *Sobol' indices* and the total effect index S_{T_i} have been selected. These are part of the *global* SA methods and are able to correlate the output variation with the variation in the factors exploiting statistical means and usually adopting a sampling approach. A sensitivity method is said to be global if all parameters are simultaneously varied and sensitivity is evaluated over the range of each factor [20]. *Sobol' indices* have been constructed studying a special representation of integral scalar function f. What Sobol has provided in [24] is presented here:

$$f = f_0 + \sum_{s=1}^{n} \sum_{i_i=1<\ldots<i_s}^{n} f_{i_1 \ldots i_s}\left(x_{i_1}, \ldots, x_{i_s}\right), \qquad i = 1 \ldots n \tag{2}$$

where $1 \leq i_1 < \ldots < i_s \leq n$ and n is the number of factors x_i. Formula (2) can be expanded as

$$f = f_0 + \sum_{i=1}^{n} f_i\left(x_i\right) + \sum_{i<j}^{n} f_{ij}\left(x_i, x_j\right) + \ldots + f_{1,2,\ldots,n}\left(x_1, x_2, \ldots, x_n\right), \qquad i = 1 \ldots n \tag{3}$$

For each component of the function f the summands in (2) are 2^n.

Assuming that all the analysed function f is squared integrable, then all the $f_{i_1 \ldots i_s}$ are squared integrable as well. The *Sobol' indices* are identified after having defined some constants called variances, which are obtained after having squared equation (2) and integrated the results over the interesting domain of the factor $(x_1, x_2, ..., x_n)$.

$$\int f^2(x)\,dx - f_0^2 = \sum_{s=1}^{n} \sum_{i_i=1<\ldots<i_s}^{n} \int f_{i_1 \ldots i_s}^2 \tag{4}$$

The sought variances for each function f are given by the constants

$$V = \int f^2(x)\,dx - f_0^2 \tag{5}$$

$$V_{i_1 \ldots i_s} = \int f_{i_1 \ldots i_s}^2 dx_{i_1} \ldots dx_{i_s} \tag{6}$$

and it follows that

$$V = \sum_{s=1}^{n} \sum_{i_i=1<\ldots<i_s}^{n} V_{i_1 \ldots i_s} \tag{7}$$

The reason for which V and $V_{i_1 \ldots i_s}$ are called variances is due to the fact that they would actually be so for the functions f and $f_{i_1 \ldots i_s}$ if the factors x were randomly *uniformly* distributed in the domain of interest.

The *Sobol' indices* for each function f and for the factors $(x_1, x_2, ..., x_s)$ are finally given by

$$S_{i_1 \ldots i_s} = \frac{V_{i_1 \ldots i_s}}{V} \tag{8}$$

which are all non-negative leading to the result

$$\sum_{s=1}^{n} \sum_{i_i=1<\ldots<i_s}^{n} V_{i_1 \ldots i_s} = 1 \tag{9}$$

Sobol' indices are extremely powerful and can be adopted for three different types of problems exploiting the fact that the higher is the value of the index $S_{i_1 \ldots i_s}$, the more important are the factors $(x_1, x_2, ..., x_s)$ and their integration. The three problems are:

1. ranking of variables
2. identifying non-essential variables
3. detecting high order members in (2).

The selection of the parameters more significant to perform UQ in terms of the branches presented in subsection 2.3, is a problem that belongs to the first two points above-mentioned and the main effect S_i and total effect index S_{T_i}, introduced by Saltelli [20]-[23], have been determined. Saltelli has emphasized the importance of S_{T_i}, which measures the total effects (i.e. first and higher order iteration) of factor x_i, especially in the presence of a huge number of factors.

The sum of these indices $\sum_{i=1}^{n} S_{T_i}$ must be greater or equal to 1. The equality occurs only in the case of a perfect additive model and in that case $\sum_{i=1}^{n} S_i = 1$.

The function $f_{i_1 \ldots i_s}$ and the main S_i and total effects S_{T_i} are obtained as [21]

$$\begin{aligned} f_0 &= E(Y) \\ f_i &= E_{\mathbf{X}_{\sim \mathbf{i}}}(Y|\, X_i) - E(Y) \\ f_{ij} &= E_{\mathbf{X}_{\sim \mathbf{ij}}}(Y|\, X_i, X_j) - f_i - f_j E(Y) \end{aligned} \tag{10}$$

$$\begin{aligned} S_i &= \frac{V_{X_i}(E_{\mathbf{X}_{\sim \mathbf{i}}}(Y|\, X_i))}{V(Y)} \\ S_{T_i} &= \frac{E_{\mathbf{X}_{\sim \mathbf{i}}}(V_{X_i}(Y|\, \mathbf{X}_{\sim \mathbf{i}}))}{V(Y)} = 1 - \frac{V_{\mathbf{X}_{\sim \mathbf{i}}}(E_{X_i}(Y|\, \mathbf{X}_{\sim \mathbf{i}}))}{V(Y)} \end{aligned} \tag{11}$$

where Y stands for the function of interest f, $E_X(\cdot)$ and $V_X(\cdot)$ are the mean and variance of argument $(\cdot)$ over $\mathbf{X_i}$, while $E_{\mathbf{X}_{\sim \mathbf{i}}}(\cdot)$ and $V_{\mathbf{X}_{\sim \mathbf{i}}}(\cdot)$ are the mean and variance of all factors but X_i.

In order to efficiently perform the SA, a computational approach that allows a simultaneous computation of S_i and S_{T_i} has been adopted and the indices are evaluated using a surrogate model (the Blind Kriging) developed for each selected output u, trained and validated with a suitable number of sampling points, adopting Sobol' sequences (also known as LP_τ sequences) as the quasi-Monte Carlo algorithms. An analytical evaluation of such indices is feasible just for simple systems, which is not the case here. The considered numerical computation has been presented by Saltelli [21] [25] and consists of using two independent $N \times k$ matrices $\mathbf{A}$ and $\mathbf{B}$, whose rows and columns are the considered sampling points and design variables respectively, and a third $(N \cdot k) \times k$ matrix $\mathbf{C}$ that is constructing from the previous ones. Each $\mathbf{C^{(i)}}$ block $(i = 1 \ldots k)$ of the matrix $\mathbf{C}$ can be formed:

1. by all columns of $\mathbf{A}$ except the $i - th$ column, which is taken by $\mathbf{B}$
2. by all columns of $\mathbf{B}$ except the $i - th$ column, which is taken by $\mathbf{A}$

Whatever case is chosen, $N \times (k + 2)$ model evaluations are required to determine the sought indices. In [21] Saltelli showed that with the first algorithm a higher rate of convergence is achieved if the following formula for $V_{X_i}(E_{\mathbf{X}_{\sim \mathbf{i}}}(Y|\, X_i))$ and $E_{\mathbf{X}_{\sim \mathbf{i}}}(V_{X_i}(Y|\, \mathbf{X}_{\sim \mathbf{i}}))$ are adopted to calculate S_i and S_{T_i}, respectively.

$$\begin{aligned} V_{X_i}(E_{\mathbf{X}_{\sim \mathbf{i}}}(Y|\, X_i) &= \frac{1}{N} \sum_{j=1}^{N} f(\mathbf{B})_\mathbf{j} (\mathbf{f}(\mathbf{C^{(i)}})_\mathbf{j} - \mathbf{f}(\mathbf{A})_\mathbf{j}) \\ E_{\mathbf{X}_{\sim \mathbf{i}}}(V_{X_i}(Y|\, \mathbf{X}_{\sim \mathbf{i}})) &= \frac{1}{2N} \sum_{j=1}^{N} (f(\mathbf{A_j}) - \mathbf{f}(\mathbf{C^{(i)}})_\mathbf{j})^\mathbf{2} \end{aligned} \tag{12}$$

The last term to be calculated is the total variance V and, since it is function of f_0^2, a formula for f_0 is also required. The existence of three possible equations for V and four for f_0 have been

found [26], giving a total of 12 possible combinations such that:

$$\hat{f}_0^2 = \left(\frac{1}{N} \sum_{j=1}^{N} f(\mathbf{A}) \right)^2 \tag{13}$$

$$\hat{f}_0^2 = \left(\frac{1}{N} \sum_{j=1}^{N} f(\mathbf{B}) \right)^2 \tag{14}$$

$$\hat{f}_0^2 = \left(\frac{1}{2N} \sum_{j=1}^{N} f(\mathbf{A}, \mathbf{B}) \right)^2 \tag{15}$$

$$\hat{f}_0^2 = \frac{1}{N} \sum_{j=1}^{N} f(\mathbf{A}) f(\mathbf{B}) \tag{16}$$

$$\hat{V} = \frac{1}{N-1} \sum_{j=1}^{N} f^2(\mathbf{A}) - \hat{f}_0^2 \tag{17}$$

$$\hat{V} = \frac{1}{N-1} \sum_{j=1}^{N} f^2(\mathbf{B}) - \hat{f}_0^2 \tag{18}$$

$$\hat{V} = \frac{1}{2(N-1)} \sum_{j=1}^{2N} f^2(\mathbf{A}, \mathbf{B}) - \hat{f}_0^2 \tag{19}$$

In the present analysis, all of these combinations have been considered and compared in order to find out the one that gives the most coherent result with respect to the stated properties of the indices and with the lowest computational time for convergence.

Sobol' indices can be evaluated using surrogate models [5] of the selected outputs u, trained with a suitable number of sampling points. These surrogate models are related to $B+1$ points on each first set of identified branch (one for all the considered sampling points, subsection 2.3); these points are obtained by dividing each identified branch in an equal number of intervals B.

In order to consider the importance of the design parameters, and so determine the Sobol' indices, it is important to select suitable objective functions u, used as 'objective' functions for the Sobol' indices. For the landing gear system the objective functions u have been defined having fixed the two parameters that have to be considered as operating ones due to their importance for a landing gear system: the forward velocity V and the vertical force on the landing gear F_z. The qualitative change in the branches can be captured if the objective functions describe both variation in the **shape** and **translation** of the interesting branches. Thus, two kinds of indices have been selected:

1. for each determined segment on the analysed branches, the approximated slope is taken as an objective function to capture change in the **shape** of the analysed branch

$$f_{1b_{i_1 \ldots i_s}}(p_{i_1 \ldots i_s}) = \left. \frac{\partial F_z}{\partial p_{i_1 \ldots i_s}} \right|_b \simeq \left. \frac{\Delta F_z}{\Delta p_{i_1 \ldots i_s}} \right|_b \qquad b = 1 \ldots B \quad 1 \leq i_1 < \ldots < i_s \leq N_P \tag{20}$$

[5] Blind Kriging surrogate models have been adopted.

2. at the first determined Hopf bifurcation point, i.e. at which the continuation has been switched in two parameters, the velocity V_1 is considered as an objective function to discuss **translations** of the interesting branch

$$f_{2_{i_1 \ldots i_s}}\left(p_{i_1 \ldots i_s}\right) = V_1\left(p_{i_1 \ldots i_s}\right) \qquad 1 \leq i_1 < \ldots < i_s \leq N_P \tag{21}$$

where N_P is the number of the analysed parameters. Thus, in total $B+1$ objective functions are considered and the first B have to be considered as a whole since since they describe the change in the **shape** of the interesting branch; the mean in terms of all the intervals B has been considered for each branch. If a significant topology variation of the bifurcation diagram occurs changing a particular parameter, then this should be considered as an operating parameter.

Once the SA is accomplished, then the UQ can be performed in terms of the most influential uncertain parameters. In the following subsection the adopted new methodology is presented. It is based upon the same principles characterizing the already tested technique developed by the author to predict and propagate parametric uncertainties up to correlated time-history quantities [13].

3.2 UNCERTAINTY QUANTIFICATION

The methodology for propagating parameter uncertainties belongs to the so called sampling-based analysis: the Singular Value Decomposition (SVD) and/or High Order Singular Value Decomposition (HOSVD) have been adopted both to speed up the process and to store data. The SVD/HOSVD is adopted to accomplish the feature extraction and selection, a critical step in machine learning problems [27]. The other key to speed up the process is to consider surrogate models rather than running the numerical model. The surrogate models have been trained and validated using the Latin Hypercube Sampling (LHS) method [28].

The proposed UQ can be divided in three parts as summarized in Figure 4.

1. Application of SVD/HOSVD
2. Surrogate Model Selection
3. Uncertainty Quantification

In what follows each part of the developed technique for UQ is detailed.

Application of SVD/HOSVD The SVD is defined as: *for every matrix* $\mathbf{A} \in \mathbb{R}^{\mathrm{m}\times\mathrm{n}}$ *there exist two orthogonal matrices* $\mathbf{U} \in \mathbb{R}^{\mathrm{m}\times\mathrm{m}}$ *and* $V \in \mathbb{R}^{\mathrm{n}\times\mathrm{n}}$ *and a diagonal matrix* $\mathbf{\Sigma} \in \mathbb{R}^{\mathrm{m}\times\mathrm{n}}$*, whose diagonal collects the non-negative singular values* $\lambda_1 \geq \lambda_2 \geq \ldots \geq \lambda_{\min n,m} \geq 0$*, such that* $\mathbf{A}$ *can be decomposed as* $\mathbf{A} = \mathbf{U}\mathbf{\Sigma}\mathbf{V}^{\mathbf{T}}$.

In order to reduce the dimension of a problem, $\mathbf{A_T}$, a truncated SVD can be considered. It is the matrix obtained considering only the columns of $\mathbf{U}$ and $\mathbf{V}$ (i.e. the singular vectors) related to the k highest singular values; usually the non-zero singular values are chosen although this can sometimes be difficult to do in practice, and therefore the most significant terms are retained. Several methods have been investigated (Guttman-Kaiser criterion, Captured Energy, Cattells Scree test) to identify the correct rank for truncated SVD and the Captured Energy has been adopted due to the good results recently obtained [29]. This method consists of selecting enough singular values such that the sum of their squares is a certain percentage T of the total

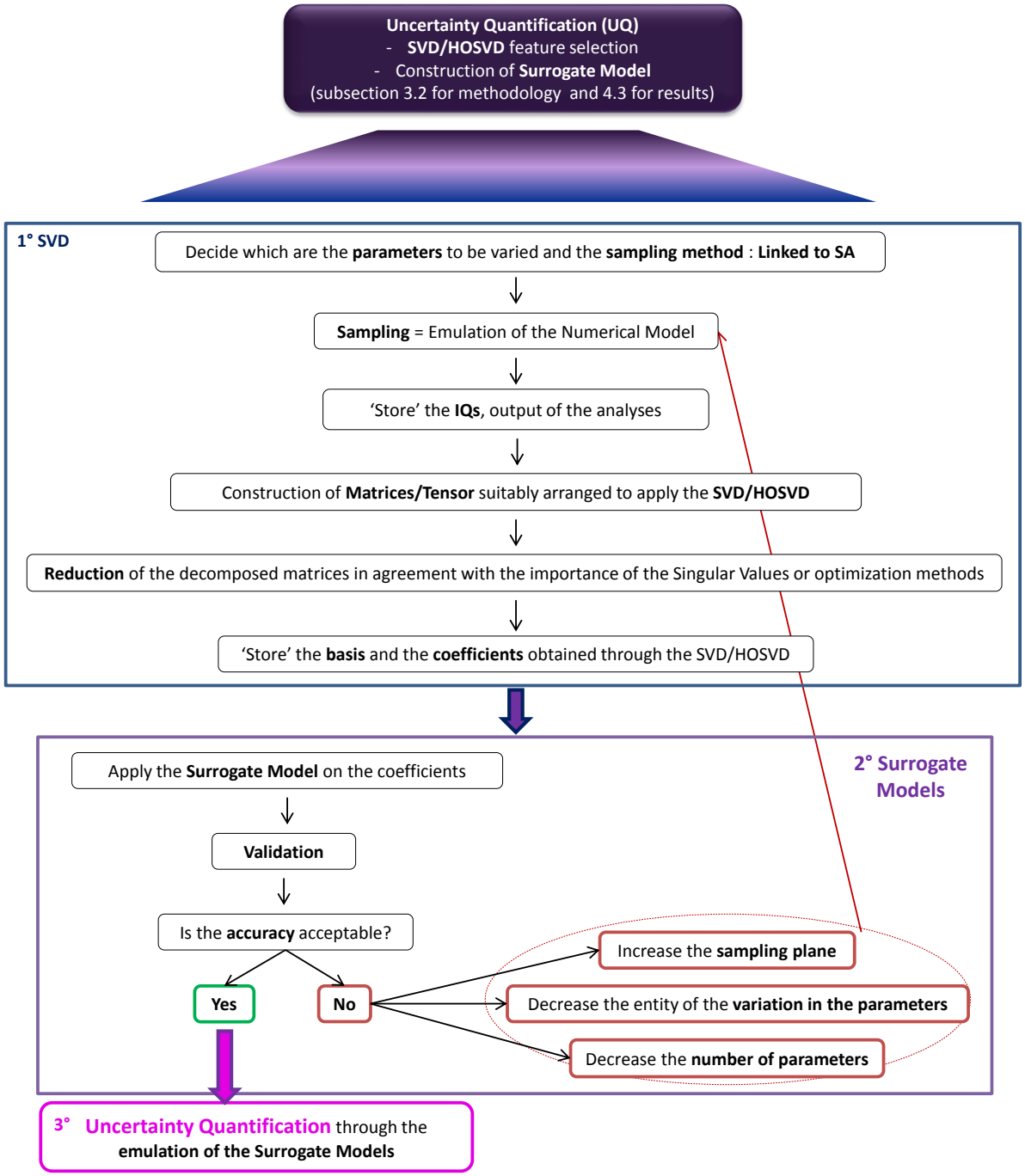

Figure 4: Flow chart for the Uncertainty Quantification.

sum of the squared values. The reason for such a decision is that the resulting matrix 'capture' $T\%$ of the Frobenius norm of the full matrix, that is correlated with the energy.

In the aeronautics field, the SVD has been used for over 30 years, applied to a range of different purposes including system identification and modal analysis. Recently, Sarkar et al.[30] have developed, demonstrated and tested a SVD-based method for symbolic design optimiza-

tion problem reformulation. Such a method has been applied to Hydraulic Cylinder Design and Aircraft Concept Sizing. Armstrong [31] used such a technique both to accomplish a down-selection procedure in terms of loads, identifying a suitable set of unit loads, and also to predict the response of a structure faster.

Recently a new approach for feature extraction has been introduced, the High Order Singular Value Decomposition (HOSVD), which exploits tensorial operators and not only matrices. This can be useful in the presence of output, such as the branches of bifurcation diagrams, to be analysed in terms of a high number of parameters.

Given a tensor $\mathcal{A} \in \mathbb{R}^{\mathrm{I}_1 \times \mathrm{I}_2 \ldots \times \mathrm{I}_\mathrm{D}}$ the HOSVD can be mathematically expressed as [32] [33]:

$$\mathcal{A} = \mathcal{S} \times_{\mathbf{1}} \mathbf{U^1} \times_{\mathbf{2}} \mathbf{U^2} \ldots \times_{\mathbf{D}} \mathbf{U^D} \tag{22}$$

where $\mathcal{S}$ is the core tensor and $\dim \mathcal{S} = I_1 \times I_2 \ldots \times I_D$, $\dim \mathbf{U^i} = I_i \times I_i$.

As for the SVD, the HOSVD gives the possibility in reducing the dimensions of the problem, capturing the best rank reduction for the analysed tensor. We have used a tool in Matlab to perform the HOSVD [34] and two rank approximations, the so called truncated multilinear singular value decomposition (mlsvd) and the one that uses a non linear least square method (lmlra) (for further information see [34]).

In the methodology the SVD/HOSVD is adopted for feature extraction by fixing a basis and then using other coefficients to obtain the required information. If the SVD is considered, the basis is given by the product of the diagonal matrix and the matrix containing the right singular vectors, namely $\mathbf{\Sigma_k V_k^T} \in \mathbb{R}^{\mathrm{k} \times \mathrm{m}}$; the coefficients that vary with respect to the design parameters are the terms of the matrix of the left singular vectors $\mathbf{U_k}$. If the HOSVD is applied, the basis is $\mathcal{S}_\mathbf{k} \times_{\mathbf{2}} \mathbf{U_k^2} \ldots \times_{\mathbf{D}} \mathbf{U_k^D}$ and the coefficients of the matrix related to the selected points is $\mathbf{U^1}$ if the 1^{st} dimension of the tensor $\mathcal{A}$ is the one related to the sampling plane.

The parameters to be varied are those selected through the SA and the numerical model has to be run at each sampling point (both training and validation). Having saved all of the required outputs, either a matrix for each IQ or a tensor for all the selected IQs is constructed. For example in the validated test case, the forward velocity V and the vertical force F_z, characterizing each sought Hopf bifurcation (subsection 2.3), have been selected as IQs. The matrix, defined for each IQ and to which the SVD is applied, has as many rows as the number of uncertain parameter variations (D) and as many columns as the number $B + 1$ of points selected for all the analysed branches (as already presented for SA in subsection 3.1). The tensor, to which the HOSVD is applied, has the first dimension related to the the number of uncertain parameter variations (D), the second and third dimensions for the values of the forward velocity V and the vertical force F_z at the selected $B + 1$ points of each branch.

The SVD is applied to each IQ matrix and a basis and set of coefficients can be related to each IQ, while the HOSVD is applied to the whole tensor and just one basis and a set of coefficient is related to the IQs. The two bases for the computations are:

- $\mathbf{\Sigma_k V_k^T}$, whose dimensions are (K) x $(B + 1)$, where K is the number of singular values that are retained
- $\mathcal{S}_\mathbf{k} \times_{\mathbf{2}} \mathbf{U_k^2} \times_{\mathbf{3}} \mathbf{U_k^3}$, whose dimensions has been reduced as (K) x $(B+1)$ x (2) with $K < D$

In both cases the rank approximation is assumed not to change throughout the design space. Consequently, the variation of the pairs (V,F_z) at each Hopf bifurcation for a specific i-th sampling point can be simply identified by multiplying the respective row vector of coefficient $(\mathbf{U_k})_\mathbf{i}$ or $(\mathbf{U_k^1})_\mathbf{i}$ by the fixed basis $\mathbf{\Sigma_k V_k^T}$ or $\mathcal{S}_\mathbf{k} \times_{\mathbf{2}} \mathbf{U_k^2} \times_{\mathbf{3}} \mathbf{U_k^3}$.

Surrogate Model Selection After having identified the matrices or tensor, surrogate models of each of the K columns in the $\mathbf{U}$ or $\mathbf{U^1}$ matrix can be developed in order to enable the UQ of the IQs. Approaches often used are Kriging based methods, Neural Network, Regression Tree and Polynomial Radial Basis Functions; the Blind Kriging method [35] [36] [37] is the one that gives the best results and has been adopted also for the UQ.

Uncertainty Quantification Using the reduced order surrogate models, the efficient generation of bounds for the first set of delimitation branches (see subsection 2.3 to the occurrence of LCOs in a landing gear system have been shown.

The sought bounds can be determined in three different, but coherent, ways using the trained and validated surrogate models:

1. Extreme values adopted by the pair (V, F_z) at each $b-th$ point on the analysed branches.

2. Lower and upper bounds related to two fixed lower and upper quantiles (for instance 0.1 and 0.9). In order to keep the correlation between the IQs, all four possible combinations of correlated IQs need to be considered i.e. [$IQ1(q = 0.1)$ vs $IQ2(q = 0.1)$, $IQ1(q = 0.1)$ vs $IQ2(q = 0.9)$, $IQ1(q = 0.9)$ vs $IQ2(q = 0.1)$, $IQ1(q = 0.9)$ vs $IQ2(q = 0.9)$]. For each quartet of points, related to a specific point on the sought branch, a rectangle in the 2D space that includes all the possible correlated IQs that can occur at that point, provides the required range of quantile-bounds within the defined rectangle. The overall quantile bounds are simply found by the outer curve of all the four quantile-branch combinations.

3. Graphical description of a discrete joint probability distribution in terms of the pair (V, F_z) at each selected $b - th$ point on the analysed branch. This representation can be obtained dividing in an arbitrary number of rectangles the box defined, at each interesting point $b-th$ of the sought delimitation, by the maximum range acquired by each IQ (V and F_z). In practice, at each point and in each sub-rectangle of the defined box, the discrete probability function is given by the ratio between the number of occurrences of the pair (V, F_z) in the considered sub-rectangle and the total occurrences in the whole box. This stratagem is needed since the data, obtained through the continuation, are discrete and it is improbable that they acquire the same values changing sampling points.

3.3 ISOLATED BRANCHES AND SUBCRITICAL HOPF BIFURCATION

In order to investigate whether Hopf bifurcations occur for values of the force and velocity less than the ones characterizing the first set of identified branches, a periodic orbit continuation has been considered starting from points that have been determined through AUTO and that are equal to or occur just after the one selected for the UQ. In this way, if for some point a Hopf bifurcation is identified for less values of those acquired by the pair (V, F_z) at the point at which the periodical continuation is started, then it has to be checked if the found Hopf bifurcation belongs to a new branch or is a previous one on the already found branch. A simple stratagem to automatically accomplish this point is to look at the percentage difference in terms of the velocity and force characterizing the Hopf bifurcation and the nearest point on the already found branch: the 'new found' Hopf bifurcation belongs or not to a new branch depending on whether the percentage error is greater or less than a fixed tolerance (for instance 1%). The tolerance is necessary to be considered due to the inherent discrete data.

Finally, the occurrence of subcrtical Hopf bifurcation can be checked looking at the stability of the first points found through periodical continuation. If they are all stable then only supercritcal Hopf bifurcations occur, otherwise subcritical Hopf bifurcation happens. AUTO determines whether a LCO is stable or not calculating the Floquet multiplier [15].

3.4 ERROR METRICS

In order to validate the surrogate models adopted in SA and UQ and the determined confidence bounds, the mean absolute percentage error (MAPE) has been adopted as the error metric. Letting z be the general actual output and $\hat{z}$ the predicted output to be validated, the MAPE is defined as

$$MAPE = \frac{1}{N}\sum_{i=1}^{N}\left|\frac{\hat{z}-z}{z}\right| \tag{23}$$

In the case study, N is:

- the number of validation points if the validation of the surrogate model used in SA and UQ is considered;
- the number of points $B+1$, adopted to describe the sought delimitation, if the validation of the confidence bounds is performed

B and $B+1$ values of $MAPE$ are obtained for the validation of the surrogate models adopted in SA and UQ, respectively. Thus, a further mean in all the discrete partial derivatives B or number of points $B+1$ on each branch can be considered if a global measure of validation is desired, that is for instance for SA

$$\overline{MAPE} = \frac{1}{B}\sum_{i=1}^{B} MAPE \tag{24}$$

Finally, the confidence bounds have been validated considering the results given by Monte Carlo Simulation (MCS) as the truth.

4 RESULTS

In this section the results obtained applying the new methodology to the landing gear are provided. First the approach adopted to describe the branches (both in SA and UQ) is presented graphically. Then the validation of the surrogate models adopted in the SA and the main and total effect indices are discussed. Finally, the validation of the surrogate models considered in the UQ and the confidence bounds determined with three approaches for the sought delimitations are presented. A discussion about the possible occurrence of subcritical Hopf bifurcation and Hopf bifurcation at values of (V, F_z) less than those characterizing the identified branches is also provided.

4.1 DESCRIPTION OF INTERESTING BRANCH

The delimitation of the occurrence of LCO in the 2-parameter space (V,F_z), is described considering a fixed number of points $B+1$ for all the considered sampling points (both training and validation). As already stated in subsection 3.1, these points are obtained dividing each branch into B equal intervals. In this subsection, illustrations of the description adopted for the sought branches is shown (Figure 5).

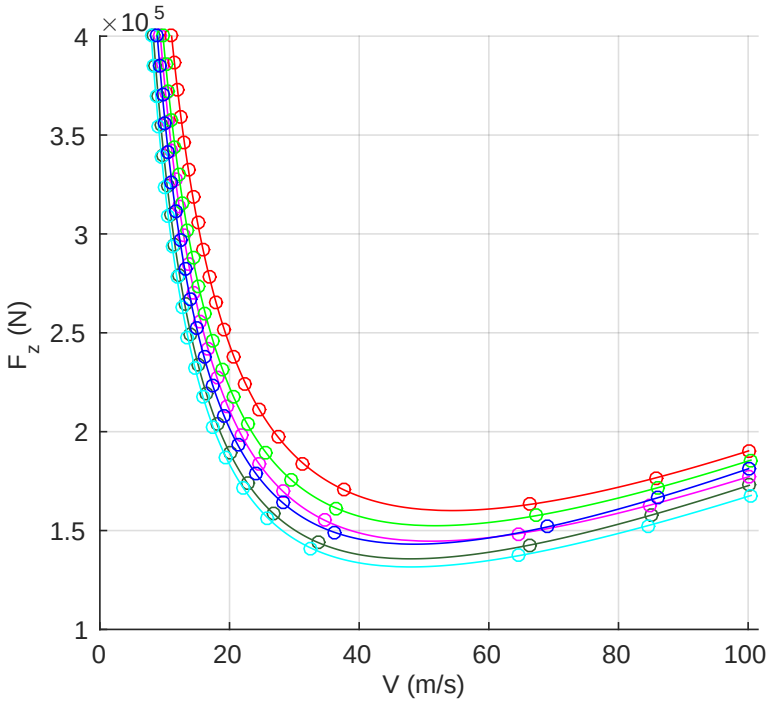

Figure 5: Example of the desciption adopted for the sought branches to perform both the Sensitivity Analysis and the Uncertainty Quantification. In this example B is fixed equal to 20 and each line is a 2-parameter continuation of Hopf bifurcations obtained at a particular sampling point.

4.2 SENSITIVITY ANALYSIS

The parameters and relative range considered to perform the SA, i.e. calculate the main and total effect indices, are shown in Table 1. Log-uniform and uniform probability distributions have been adopted if the variation of the analysed parameter is greater or less of one order of magnitude, respectively. This choice is due to the lack of information about the parametric uncertainty [20]. For the sake of completeness, Table 1 shows which probability distribution has been adopted for each parameter.

The parameters that have not been considered in the SA are those related to:

- the longitudinal DoF β, since the side stay angle μ (also known as horizontal attachment point orientation angle) has been fixed equal to zero (as if it was a nose landing gear) and in such a configuration the longitudinal dynamic is less influential;
- the parameters characterizing the adopted straight tangent model for the tyre, since the whole model itself is made on an assumption and so would require an uncertainty analysis on its own;
- geometrical distances that are well defined during the design process and difficult to change during the life of an aircraft, for instance the half track width or the caster length.

In order to determine the desired main and total effect indices, the dimension N of the matrices characterizing Saltelli's technique (subsection 3.1) has been fixed equal to 15; thus 195 continuations in V and F_z have been computing using AUTO to identify the first set of branches,

Parameter	Label	Maximum	Minimum	Units	PDF
stiffness coefficient of ψ DoF	k_ψ	963000	837000	N m rad^{-1}	log-uniform
stiffness coefficient of δ DoF	k_δ	6420000	5580000	N m rad^{-1}	log-uniform
inertia of ψ DoF	I_ψ	107	93	kg m^2	uniform
inertia of δ DoF	I_δ	428	372	kg m^2	uniform
damping coefficient of ψ DoF	c_ψ	1284	1116	N m s rad^{-1}	log-uniform
damping coefficient of δ DoF	c_δ	535	465	N m s rad^{-1}	log-uniform
radius of the left wheel	rL	0.59	0.5487	m	uniform
radius of the right wheel [6]	rR	0.59	0.5487	m	uniform
tyre relaxation length	L	0.5671	0.4929	m	uniform
length of contact region	h	0.2889	0.2511	m	uniform
vertical stiffness of tyres	k_t	1716280	1491720	N m^{-1}	log-uniform

Table 1: Parameters and the range of values adopted in the Sensitivty Analysis

the locus of Hopf bifurcation in the (V, F_z) parameter space (subsection 2.3). Then, fixing B, the number of the discrete partial derivatives, equal to 20, the obtained data have been post-processed identifying the pairs (V, F_z) related to the points $B + 1$ of each branch. Thus, surrogate models for the selected objective functions u (slope and velocity, subsection 3.1 eq. (20) and (21)) have been constructed adopting Sobol' sequences as a quasi-Monte Carlo sampling plane.

The obtained surrogate models have been validated considering 10 validation points and the $MAPE$ (and mean of $MAPE$ in all the slopes for the first objective functions, section 3.4) are shown in Tables 2 and 3. It is apparent that the trained surrogate model replicates the actual objective functions with extremely high accuracy.

Using the surrogate models, Saltelli's technique has been adopted to evaluate the main and total effect indices, and all the 12 combinations to determine the total variance V have been considered (subsection 3.1). For the sake of clarity, these have been numbered as shown in Table 4 (see section 3.1 for the expressions).

The comparison is done considering different numbers of evaluations of the surrogate models to test the performance in terms of convergence. The main and total effect indices of all the defined objective functions empathize that the best combination is either the 4^{th} or 8^{th} one. This result is shown here in Figures 6 and 7, which provide for the sake of conciseness just the comparison for the sum of the main and total indices related to the 19^{th} slope. Looking at the

Index Slope	$MAPE$ slope	Index Slope	$MAPE$ slope
1	$2.06 \cdot 10^{-3}$	11	$5.80 \cdot 10^{-3}$
2	$8.67 \cdot 10^{-4}$	12	$6.81 \cdot 10^{-3}$
3	$2.93 \cdot 10^{-3}$	13	$7.72 \cdot 10^{-3}$
4	$1.68 \cdot 10^{-3}$	14	$1.08 \cdot 10^{-2}$
5	$3.83 \cdot 10^{-3}$	15	$1.11 \cdot 10^{-2}$
6	$3.07 \cdot 10^{-3}$	16	$1.55 \cdot 10^{-2}$
7	$4.35 \cdot 10^{-3}$	17	$5.11 \cdot 10^{-2}$
8	$4.58 \cdot 10^{-3}$	18	$3.94 \cdot 10^{-1}$
9	$4.74 \cdot 10^{-3}$	19	$3.44 \cdot 10^{-2}$
10	$3.95 \cdot 10^{-3}$	20	$1.04 \cdot 10^{-2}$

Table 2: $MAPE$ of the objective functions in terms of the slope.

$\overline{MAPE}$ slope	$MAPE$ velocity
$2.9 \cdot 10^{-}2$	$6.95 \cdot 10^{-}2$

Table 3: Mean of $MAPE$ of the objective functions in terms of the slope and $MAPE$ of the objective function in terms of the velocity at the first identified point.

4^{th} or 8^{th} combinations, it can be noticed that the system is almost additive for the considered parameter-variation: all the defined objective functions [7] present $\sum_{i=1}^{N} S_{T_i}$ and $\sum_{i=1}^{N} S_i$ are respectively greater and less than 1 as they have to be (subsection 3.1), but only just.

Finally, considering the 4^{th} combination, the main and total effect indices are evaluated for both the considered objective functions in order to select the parameters to be adopted for the UQ, i.e. those more influential; both the objective functions show that I_ψ, c_ψ and L are the most influential parameters.

This is illustrated in the bar plot of the total effect for all the parameters (Figure 8). Always for the sake of conciseness, just the mean [8] of the adopted index related to the slope-objective

[7] Here, just the results for indices related to the 19^{th} slope are shown.

[8] As stated in subsection 3.1 the mean for all the B evaluated indices in terms of slope can be considered as a whole information.

Combination	eq. f_0^2 and V		Combination	eq. f_0^2 and V	
1	13	17	7	15	18
2	14	17	8	16	18
3	15	17	9	13	19
4	16	17	10	14	19
5	13	18	11	15	19
6	14	18	12	16	19

Table 4: Combinations adopted to identify the best espression to be used for the total variance V.

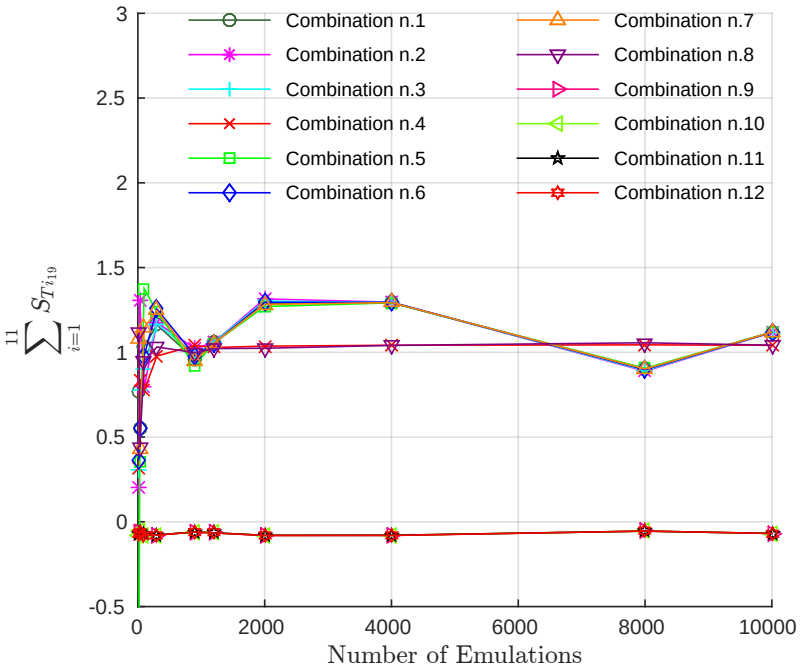

Figure 6: Comparison of 12 different evaluations of the total variance V considering the sum of the total effects S_{T_i} of the 19^{th} slope-objective function.

functions is shown, that is

$$\overline{S}_{T_i} = \frac{1}{B}\sum_{b=1}^{B}(S_{T_i})_b \tag{25}$$

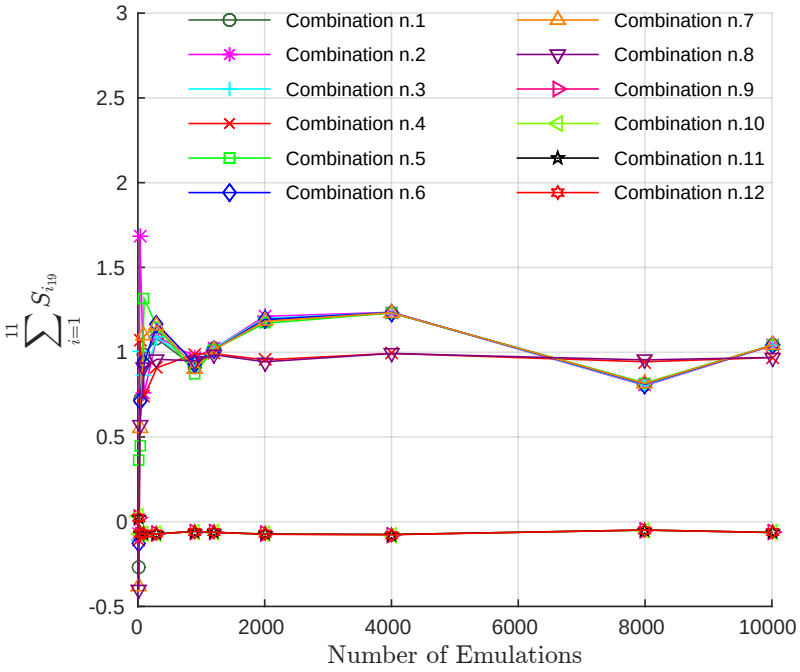

Figure 7: Comparison of 12 different evaluations of the total variance V considering the sum of the main effects S_i of the 19^{th} slope-objective function.

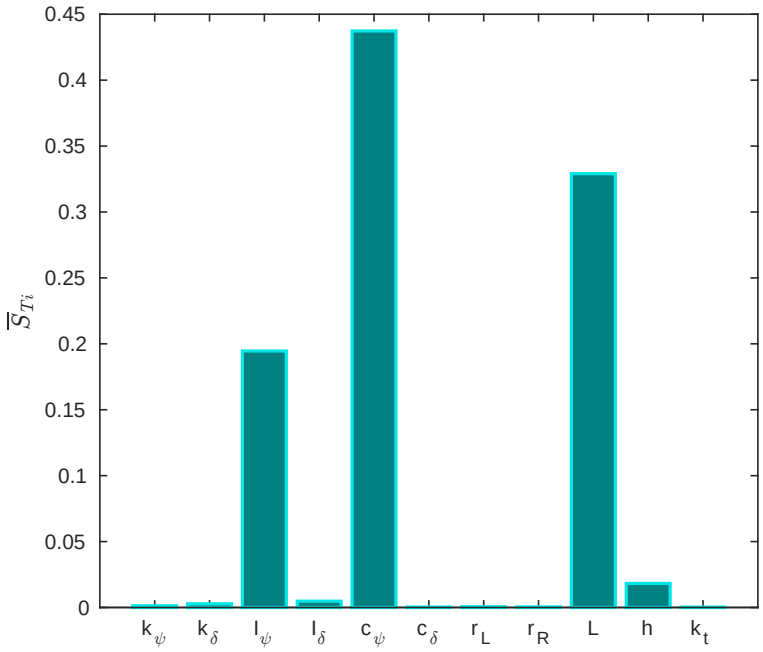

Figure 8: Comparison of the influence of each parameter on the output considering the mean of the total effect S_{T_i} related to the slope objective function.

The obtained results are totally coherent with the *shimmy* phenomenon: *shimmy* is primarily related to the tyre characteristics and, for the analysed branch, to the torsional dynamics. In fact, looking at the LCOs generated by each of the analysed point on all the determined branches, the torsional state ψ always presents the greatest amplitude and is almost in phase with the state λ of the tyre dynamics; this means that the torsional mode is the one that most participates in the LCOs. It can be also noticed that the period of the LCOs is in practice always around that characterizing the linearised torsional mode: the period of the LCOs is always about $6-7\cdot10^{-2}$ sec and the damped natural period of the linearised torsional mode is $6.76 \cdot 10^{-2}$ sec.

Keeping in mind the results given by the SA, the validation of the surrogate models and the determined confidence bounds are provided in the following subsection.

4.3 UNCERTAINTY QUANTIFICATION

The performed UQ in terms of the first set of delimitation-branches (subsection 2.3) of the occurrence of LCOs has been performed in terms of the three most influential parameters (subsection 4.2), I_ψ, c_ψ and L , whose range and probability distribution has been discussed in subsection 4.2 and shown in Table 1.

For the UQ, 31 points $(B+1)$ have been considered on all the identified branches, 100 points-LHS plane and 1000 point-LHS have been considered in order to train and validate the surrogate models, respectively.

The number of singular values to be retained in the SVD have been identified using the Captured Energy method and fixing to 99.99 the percentage T of the captured energy (subsection 3.2). 4 and 3 are the numbers of singular values retained for the matrix related to the forward velocity V and vertical force F_z, respectively; a total of 7 surrogate models are required to perform the sought UQ using the SVD. The same number of surrogate models are required if the HOSVD is applied and leads to a core tensor with dimension $7 \times 31 \times 2$. Such a decision has been drawn due to the bad results obtained adopting TensorLab [34] to find out the best rank reduction. In TensorLab the rank reduction for the mlsvd and as starting guess for the lmlra method is selected as the corner of an L-curve that represents the balance between an upper bound on the relative error and the compression ratio of a low multi-linear rank approximation of the starting tensor $\mathcal{A}$ for different core tensor sizes [34]. In the present problem, the corner of the L-curve is found for a core tensor with dimension $3 \times 3 \times 1$ and results in a bad choice for both the mlsvd and lmlra methods; errors higher than 100% are determined just at the training points. The reason for these bad results is the adoption of a reduction not constrained just in terms of the dimension related to the sampling plane, i.e. the first dimension of $\mathcal{A}$. A reduction in terms of the stated first dimension can be simply accomplished considering the first unfolding matrix $\mathbf{A}_{(\mathbf{1})}$ and using the Captured Energy method. We have decided to compare the results applying the SVD and the HOSVD with the same number of surrogate models (7).

Very good results are found for the validation of the surrogate models adopted for both the SVD and HOSVD mlsvd, while not so good for those related to the HOSVD lmlra. As stated in section 3.4 the validation has been accomplished considering $\overline{MAPE}$ as error metric; Table 5 provides such a results. Figure 9 provides an example of validation adopting the SVD and the mlsvd for the HOSVD. Only the mlsvd is shown since it has a lower error in the validation compared to the lmlra method (Table 5). For the same reason the confidence bounds have been evaluated only with the mlsvd when the HOSVD has been considered.

All the three methods presented in subsection 3.2 have been considered to deal with the confidence bounds for which the surrogate models have been evaluated considering a 1000 points-LHS sampling plane. The graphic results are shown here all together in Figure 10; for

Method	$\overline{MAPE}\%$ for V	$\overline{MAPE}\%$ for F_z
SVD	$5.61 \cdot 10^{-1}$	$1.05 \cdot 10^{-1}$
HOSVD lmlra	8.11	7.94
HOSVD mlsvd	$3.67 \cdot 10^{-1}$	$9.56 \cdot 10^{-2}$

Table 5: $\overline{MAPE}$ obtained using the SVD/HOSVD based surrogate model for V and F_z.

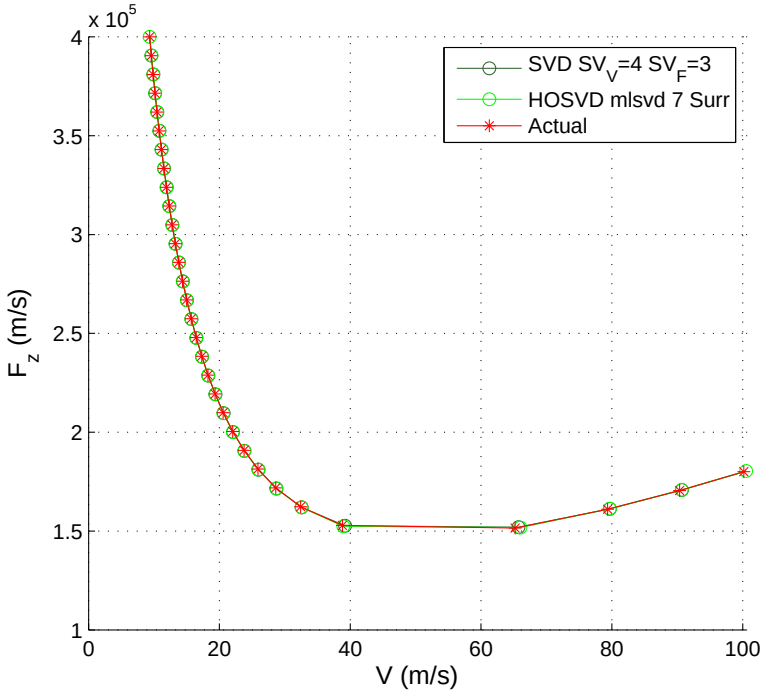

Figure 9: Validation of the Blind Kriging Surrogate models adopted to perform Uncertainty Quantification using SVD or HOSVD.

the sake of simplicity the confidence bounds shown in Figure 10 are only for the results obtained considering the SVD based method. The HOSVD gives almost the same results. As stated in subsection 3.2, considering the third method, a rectangle at each analysed point on the branch is defined and divided into sub-boxes. In the present case 6 sub-boxes have been considered and several lines (with different colors) define delimitations of indicate joint probability distributions at each rectangle. The third approach is more approximate than the others since it is based on a further discretization of the outputs and a comparison with the first and second approach is meaningless; however, it gives information about joint probability of the position of the analysed $B + 1$ Hopf bifurcation points in the 2D parameter space.

Regarding the validation, a MCS with 1000 points has been considered and the results are presented both in terms of $\overline{MAPE}$ in Tables 6a and 6b and graphically in Figures 11a (for the interval confidence bounds) and 11b (for the quantile confidence bounds). The very good

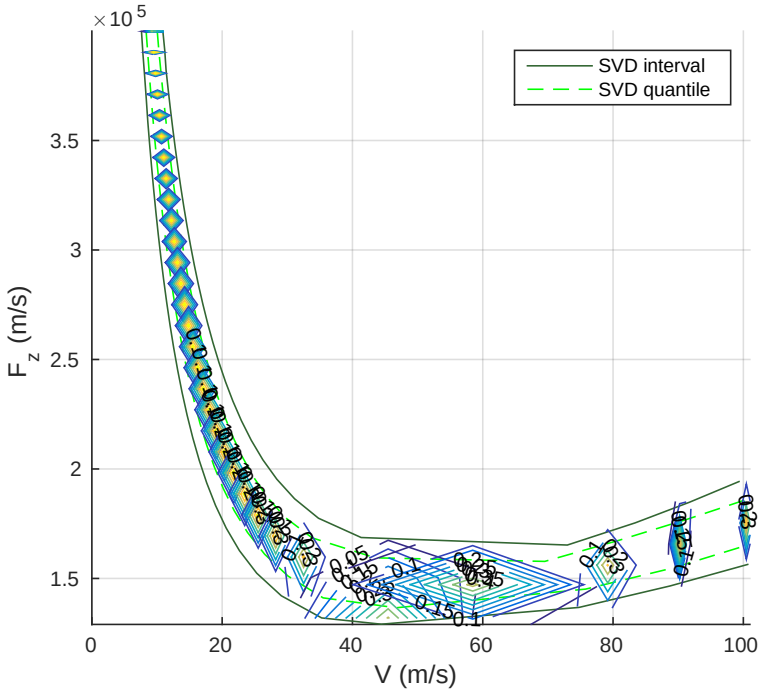

Figure 10: Confidence bounds of the delimitaion of area in which the LCO can or cannot occur, adopted using all the three methods.

accurateness achieved with both the SVD and HOSVD mlsvd based methodology is apparent. It is worthy to emphasize that the developed method involves a computational time reduction of almost 95% compared to the MCS.

Method	$\overline{MAPE}\%$ for V	$\overline{MAPE}\%$ for F_z
SVD	$9.17 \cdot 10^{-1}$	$2.25 \cdot 10^{-1}$
HOSVD mlsvd	$8.92 \cdot 10^{-1}$	$2.67 \cdot 10^{-1}$

(a) Interval confidence bounds

Method	$\overline{MAPE}\%$ for V	$\overline{MAPE}\%$ for F_z
SVD	$1.36 \cdot 10^{-1}$	$6.17 \cdot 10^{-2}$
HOSVD mlsvd	$1.08 \cdot 10^{-1}$	$6.14 \cdot 10^{-2}$

(b) Quantile confidence bounds

Table 6: $\overline{MAPE}$ obtained using the SVD/HOSVD based surrogate model for UQ.

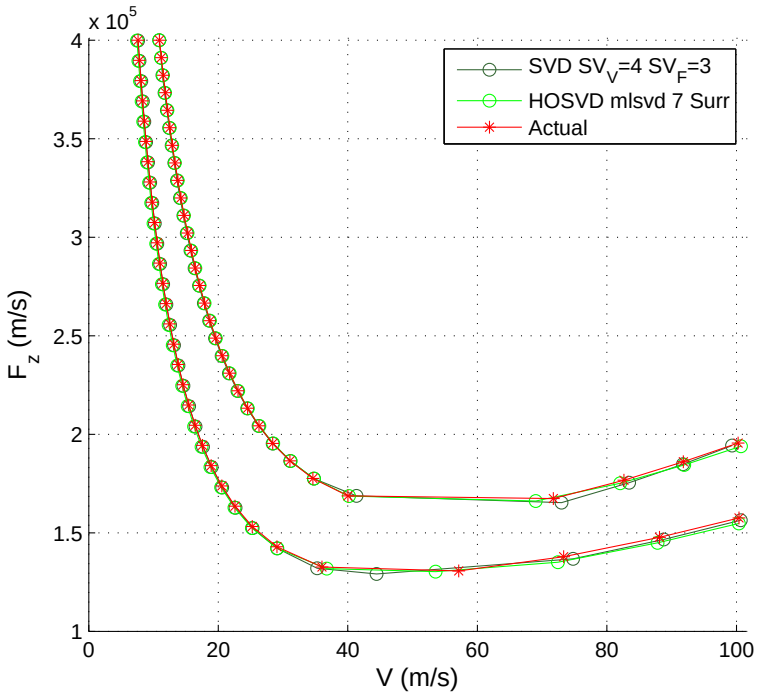

(a) Interval confidence bounds

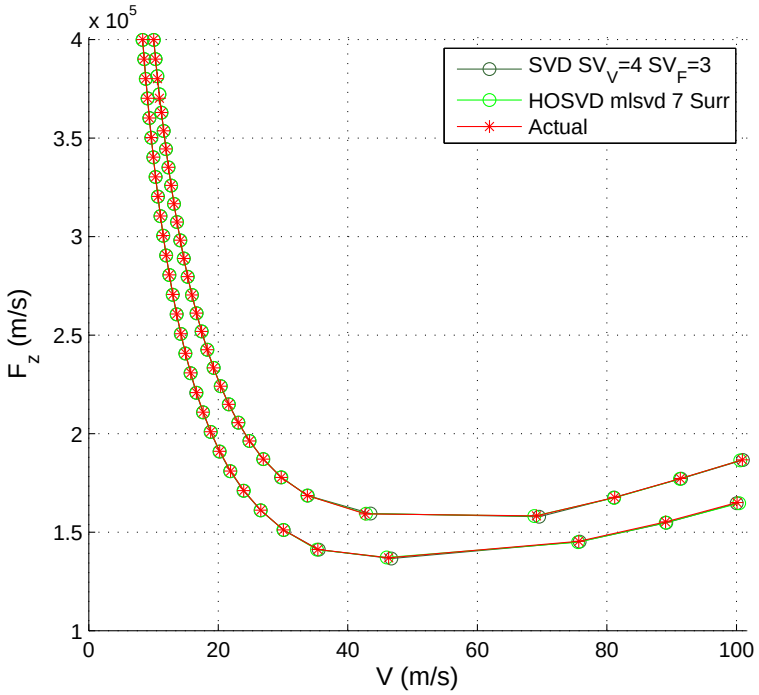

(b) Quantile confidence bounds

Figure 11: Validation of the interval and quantile confidence bounds determined with the SVD/HOSVD based developed method. The results obtained through MCS are considered as the truth.

4.4 ISOLATED BRANCHES AND SUBCRITICAL HOPF BIFURCATION

After having determined the sought confidence bounds, periodical continuation have been accomplished to check the possible occurrence of subcritical Hopf bifurcations and Hopf bifurcation at values (V, F_z) less than those characterizing the identified branches. The stability of the determined LCO can be verified just looking at the first points of the determined periodical branches and these are all stable, so no subcrical Hopf bifurcation can occur [1].

With respect to the second stated phenomena, this occurs only starting from the second Hopf bifurcation on the already identified branches, that is the second point of those that have the same values for F_z. Clearly, starting from each of these points, the first Hopf bifurcation point, which already belongs to the found branch, is identified. Thus, we can conclude that the determined confidence bounds robustly identify a separation between area in which the LCO can or cannot occur: at the right and left side of the determined bounds the LCO can and cannot occur, respectively.

5 CONCLUSIONS

The paper has presented a new methodology to robustly define confidence bounds of a bifurcation branch delimiting the region of possible occurrence of LCOs. Specific description of the branches has been proposed to perform both sensitivity and UQ. Suitable SA has been accomplished adopting main and total effect indices in order to identify the most influential parameters. Techniques for uncertainty management have been developed and applied to propagate parametric uncertainty using SVD/HOSVD and surrogate models to speed up the whole process. The determined confidence bounds for the locus of Hopf bifurcation points completely describe the sought partition since it has been proved that there is no occurrence of subcritical Hopf bifurcations and no instances of Hopf bifurcation for which the two selected parameters for the continuation of the branch-locus of Hopf bifurcation (forward velocity V and vertical force F_Z) acquire values lower than those characterising the identified branches. The validation emphasizes exceptional accuracy and a reduction of almost 95% of the total computation time required by Monte Carlo Simulations. These results have been obtained both applying the SVD and the HOSVD mlsvd (multilinear singular value decomposition) and considering a same number of surrogate models. The performed analysis has also shown that, for the HOSVD, it is preferable to consider a rank reduction just in the dimension related to the sampling plane.

6 ACKNOWLEDGMENT

This work is supported by the European Commission (EC FP7) under the Marie Curie European Industrial Doctorate Training Network 'ALPES' (Aircraft Loads Prediction using Enhanced Simulation) and also the Royal Academy of Engineering. The author wishes also to thank A. Cammarano for the exchange of opinions which is always useful.

7 APPENDIX

A NOMINAL VALUES OF PARAMETERS IN LANDING GEAR MODEL

Table 7 provides the nominal values adopted in the present paper for parameters characterizing the adopted dual-wheel landing gear model [18].

μ	0.0	rad/s
I_ψ	100.0	kg m^2
c_ψ	1200.0	N m s rad^{-1}
k_ψ	9.0×10^5	N m rad^{-1}
I_δ	400.0	kg m^2
c_δ	500.0	N m s rad^{-1}
k_δ	6.0×10^6	N m rad^{-1}
I_{β_0}	5000.0	kg m^2
c_β	2.0×10^4	N m s rad^{-1}
k_β	1.0×10^7	N m rad^{-1}
L	0.53	m
ρ	0.0	rad
ϕ_0	-0.1175	rad
L_β	2.818	m
L_δ	0.6	m
$r_L = r_R = r$	0.59	m
$h_L = h_R = h$	0.27	m
e	0.0	m
a	0.46	m
k_t	1.604×10^6	N m^{-1}
λ	1	m
c_λ	3000.0	N m^{2}rad^{-1}
k_λ	0.01	rad^{-1}
k_α	1.3256	m
α_m	0.1571	rad

Table 7: Nominal landing gear Parameters

REFERENCES

[1] S. H. Strogatz, *Nonlinear Dynamics And Chaos: With Applications To Physics, Biology, Chemistry, And Engineering (Studies in Nonlinearity)*. Westview Press, Studies in Nonlinearity, 2014.

[2] T. L. Hill, P. L. Green, A. Cammarano and S. A. Nield, *Fast Bayesian identification of multi-mode systems using backbone curves*. Journal of Aircraft, 2008, vol. 45 n. 2.

[3] G. Dimitriadis, *Continuation of Higher-Order Harmonic Balance Solutions for Nonlinear Aeroelastic Systems*. Preprint submitted to Journal of Sound and Vibration, 2014.

[4] G. Dimitriadis, G. A. Vio and J. E. Cooper, *Application of Higher-Order Harmonic Balance to Non-Linear Aeroelastic Systems*. Proceedings of the 47th AIAA/ASME/ASCE/AHS/ASC Structures, Structural Dynamics, and Materials Conference, 2006.

[5] R. Hayes and S. Marques, *Uncertainty quantification for LCO using an Harmonic Balance method*. International Forum for Aeroelasticity and Structural Dynamics (IFASD), 2013.

[6] S. K. Choi, R. V. Grandi and R. A. Canfield , *Reliability-based Structural Design*. Springer-Verlag London Limited, 2010.

[7] C. Scarth, P. Sartor, J. E. Cooper, P. Weaver and G. H. C. Silva, *Robust Aeroelastic Design of Composite Plate Wings*. 17th AIAA Non-Deterministic Approaches Conference, Orlando, Florida USA, January 5-9, 2015.

[8] G. Georgiou, A. Manan and J. E. Cooper, *Modeling Composite Wing Aeroelastic Behaviour with Uncertain Damage Severity and Material Propertiess*. Mechanical Systems and Signal Processing, Vol. 32, pp. 32-43, October, 2012.

[9] K.J. Badcock, H.H. Khodaparast, S. Timme and J.E. Mottershead, *Calculating the Influence of Structural Uncertainty on Aeroelastic Limit Cycle Response*. 52nd AIAA/ASME/ASCE/AHS/ASC Structures, Structural Dynamics, and Materials Conference,April 4-8, Denver, Colorado, 2011.

[10] Q. Ouyang, X. Chen and J. E. Cooper, *Robust Aeroelastic Analysis and Optimization of Composite Wing Under -Analysis Framework*. Journal of Aircraft, Vol. 50, pp. 1299-1305, Florida USA, 2013.

[11] P. S. Beran, C. L. Pettit and D. R. Millman, *Uncertainty quantification of limit-cycle oscillations*. Journal of Computational Physics, Vol. 217, pp. 217-247, 2006.

[12] M. E. Riley and R. V. Grandhi, *Quantification of Modeling Uncertainty in Aeroelastic Design*. 51st AIAA/ASME/ASCE/AHS/ASC Structures, Structural Dynamics, and Material Conference, Orlando, Florida USA, April 12-15, 2010.

[13] I. Tartaruga, J. Cooper, M. Lowenberg, P. Sartor, S. Coggon and Y. Lemmens, *Efficient Prediction and Uncertainty Propagation of Correlated Loads*. 56th AIAA/ASCE/AHS/ASC Structure, Structural Dynamics, and Materials Conference, Orlando, Florida USA, January 5-9, 2015.

[14] J. Guckenheimer and P. Holmes, *Nonlinear Oscillations and Dynamical Systems and Bifurcations of Vector Fields*. Springer, Series Applied Mathematical Sciences, Vol. 42, 1983.

[15] E. Doedel and B. Oldeman, *Auto-07p: Continuation and Bifurcation Software*, 2012. http://www.dam.brown.edu/people/sandsted/auto/auto07p.pdf downloaded in November, 2014.

[16] A. P. Smith, L. G. Crespo, C. A. Muñoz and M. H. Lowenberg, *Bifurcation Analysis Using Rigorous Branch and Bound Methods*. IEEE Multi-Conference on Systems and Control, 2014.

[17] ICAO Doc 8168 PANS-OPS Vol 1, http://www.ce560xl.com/files downloaded in 2015.

[18] C. Howcroft, B. Krauskopf, M. H. Lowenberg and S. A. Neild, *Influence of Variable Side-Stay Geometry on the Shimmy Dynamics of an Aircraft Dual-Wheel Main Landing Gear*. SIAM J. APPLIED DYNAMICAL SYSTEMS, Vol. 12, No. 3, pp. 11811209, 2013.

[19] http://seis.bris.ac.uk/ ec1099/, date accessed November, 2015.

[20] A. Saltelli, K. Chan and E. M. Scott, *Sensitivity Analysis*. Wiley, First edition, 2009.

[21] A. Saltelli, P. Annoni, I. Azzini, F. Campolongo, M. Ratto and S. Tarantola, *Variance based sensitivity analysis of model output. Design and estimator for the total sensitivity index*. Computer Physics Communications, Vol. 181, pp. 259-270, 2010.

[22] T. Homma & A. Saitelli, *Importance measures in global sensitivity analysis of nonlinear models*. Reliability Engineering and System Safety, Vol. 52, pp. 1-17, 1996.

[23] T. Homma & A. Saitelli, *Global Sensitivity Analysis of Nonlinear Models, Importance Measures and Sobol' Sensitivity indices*. Report EUR 16052 EN, JOINT RESEARCH CENTRE EUROPEAN COMMISSION, Environment Institute, 1994.

[24] I. M. Sobol', *Global sensitivity indices for nonlinear mathematical models and their Monte Carlo estimates*. athematics and Computers in Simulation, Vol. 55, pp. 271-280, 2001.

[25] A. Saltelli, M. Ratto, T. Andres, F. Campolongo, J. Cariboni, D. Gatelli, M. Saisana and S. Tarantola, *Global Sensitivity Analysis, The Primer*. Wiley, 2008.

[26] J. Nossent and W. Bauwens, *Optimising the convergence of a Sobol sensitivity analysis for an environmental model: application of an appropriate estimate for the square of the expectation value and the total variance*. International Environmental Modelling and Software Society (iEMSs), 2012 International Congress on Environmental Modelling and Software Managing Resources of a Limited Planet, Sixth Biennial Meeting, Leipzig, Germany R. Seppelt, A.A. Voinov, S. Lange, D. Bankamp (Eds.).

[27] K. Worden, W. J. Staszewski, J. J. Hensman, *Natural Computing for Mechanical Systems Research: A Tutorial Overview*. Mechanical Systems and Signal Processing, Vol. 25, issue 1, pp. 4-11, 2011.

[28] J. C. Helton and F. J. Davis, *Sampling-Based Methods for Uncertainty and Sensitivity Analysis*. SAND99-2240, Albuquerque, NM , Sandia National Laboratories, July, 2000.

[29] Emiliano Iuliano and Domenico Quagliarella, *Evolutionary Optimization of Benchmark Aerodynamic Cases using Physics-based Surrogate Models*. 53rd AIAA Aerospace Science Meeting, Kissimmee, Florida USA, January 5-9, 2015.

[30] S. Sarkarv, A. Dong and J. S. Gero, *Design Optimization Problem Reformulation using Singular Value Decomposition*. Journal of Mechanical Design, 2009.

[31] S. McGuinness, C. G. Armstrong, A. Murphy, J. Barron and M. Hockenhull, *Improving Aircraft Stress-Loads Evaluation and Optimization Procedures*. 2nd Aircraft Structural Design Conference, London, United Kingdom, 2010.

[32] L. De Lathauwer, B. De Moor and J. Vandewalle, *A multilinear singular value decomposition*. SIAM J.Matrix Anal. Appl., Vol. 21, n. 4, pp. 1253-1278, 2000.

[33] M. Ishteva, P. A. Absil, S. Van Huffel and L. De Lathauwer, *Best low multilinear rank approximation of higher-order tensors, based on the Riemannian trust-region scheme*. SIAM J.Matrix Anal. Appl., Vol. 32, n. 1, pp. 115-135, 2011.

[34] L. Sorber, M. Van Barel and L. De Lathauwer, *Tensorlab v2.0*. URL http://www.tensorlab.net/, January, 2014.

[35] I. Couckuyt, T. Dhaene and P. Demeester, *ooDACE toolbox, A Matlab Kriging toolbox: Getting started*. Third edition, June, 2013.

[36] R. Joseph, Y. Hung and A. Sudjianto, *Blind Kriging: A New method for Developing Surrogate models*. Journal of Mechanical Design, Vol. 130, issue 3, 2008.

[37] I. Couckuyt, A. Forrester, D. Gorissen, F. De Turck and T. Dhaene, *Blind Kriging: Implementation and performance analysis*. Advances in Engineering Software, Vol. 49, pp.1-113, 2012.

[38] I. J. M. Besselink, *Shimmy of Aircraft Main landing gears*, Technische Universiteit Delft, PhD Thesis, Department of Mechanical Engineering, 2000.

[39] J. W. L. H. Maas, *A comparison of dynamic tyre models for vehicle shimmy stability analysis*, Technische Universiteit Windhoven, PhD Thesis, Department of Mechanical Engineering, 2009.

[40] G. Somieski, *Shimmy analysis of a simple aircraft nose landing gear model using different mathematical methods*, Aerospace Science and Technology, Vol. 8, pp. 545-555, 1997.

[41] P. Thota, B. Krauskopf and M. Lowenberg, *Nonlinear analysis of the influene of tire inflation pressure on nose landing gear shimmy*, Journal of Aircraft, Vol. 47, n. 5, pp. 1697-1706, 2010.